The Emerald Research Register for this journal is available at
www.emeraldinsight.com/researchregister

The current issue and full text archive of this journal is available at
www.emeraldinsight.com/0961-5539.htm

Received January 2003
Revised February 2004
Accepted June 2004

Flow pattern transition of natural convection in a horizontal annulus with constant heat flux on the inner wall

Joo-Sik Yoo
Department of Mechanical Engineering Education, Andong National University, Andong, South Korea

Abstract

Purpose – This study considers the natural convection in a horizontal annulus with constant heat flux on the inner cylinder, and investigates the transition of flows for various Prandtl numbers.

Design/methodology/approach – The streamfunction-vorticity equation and the energy equation governing the flow and temperature field are solved with finite difference method.

Findings – Results are presented to show the transition of flow patterns with increase (or decrease) of the Rayleigh number, and a hysteresis phenomenon is observed.

Originality/value – Dual solutions are shown by using a numerical analysis in a horizontal annulus with constant heat flux on the inner wall.

Keywords Convection, Fluid power cylinders, Flow

Paper type Research paper

Nomenclature

D_i = diameter of inner cylinder
D_o = diameter of outer cylinder
g = gravitational acceleration
$\bar{h}$ = average heat transfer coefficient = $q_H/(T_{m,i} - T_o)$
k = thermal conductivity
L = gap width of the annulus = $(D_o - D_i)/2$
$\overline{Nu}$ = mean Nusselt number = $\bar{h}L/k$
Pr = Prandtl number = ν/α
q_H = constant heat flux applied on the inner cylinder
q_o = local heat flux distribution the outer cylinder
Ra = Rayleigh number = $\beta g(q_H L/k)L^3/\alpha\nu$
Ra_c = critical Ra above which dual solutions exist
Ra_{cL} = lower critical Rayleigh number
Ra_{cU} = upper critical, Rayleigh number
r = dimensionless radial coodinate
r_i, r_o = dimensionless radii of inner and outer cylinders, respectively
T = temperature
$T_{m,i}$ = mean temperature of the inner cylinder
T_o = temperature of the outer cylinder
t = dimensionless time

Greek symbols

α = thermal diffusivity
β = coefficient of thermal expansion
η = stretched coordinate in the radial direction
θ = dimensionless temperature = $k(T - T_o)/q_H L$
θ_i = dimensionless temperature distribution on the inner cylinder
$\theta_{m,i}$ = dimensionless mean temperature of the inner cylinder
ν = kinematic viscosity
ϕ = angular coordinate

International Journal of Numerical Methods for Heat & Fluid Flow
Vol. 15 No. 7, 2005
pp. 698-709

0961-5539
DOI 10.1108/09615530510613889

$\phi_{q,\max}$ = angle representing the point of maximum heat flux on the outer cylinder
ϕ_S = angle representing the location of separation point between two cells on the surface of cylinder
$\phi_{S,i}$ = ϕ_S on the inner cylinder
$\phi_{S,o}$ = ϕ_S on the outer cylinder
$\phi_{t,\max}$ = angle representing the point of maximum temperature on the inner cylinder
Ψ = dimensionless streamfunction
ω = dimensionless vorticity

1. Introduction

Natural convection in a horizontal annulus has been received much attention because of the theoretical interest and its wide engineering application such as thermal energy storage systems, cooling of electronic components and transmission cables. Comprehensive reviews on the natural convection phenomena in a horizontal annulus were presented by Kuehn and Goldstein (1976), Gebhart *et al.* (1988), and Yoo (1998).

There is no static state without fluid flow in a horizontal annulus with heated inner and cooled outer cylinders. The flow of low Rayleigh number forms a crescent-shaped eddy in which fluid rises near the inner hotter cylinder and sinks near the outer colder one (Kuehn and Goldstein, 1976). At high *Ra*, however, hydrodynamic instability (Lee and Korpela, 1983) can occur in the vertical section, and thermal instability (Busse, 1981) on the top part of thermally unstable region. The two kinds of instability yield diverse transition phenomena of the flow as the Rayleigh number increases (Yoo, 1998, 1999), which are dependent on Prandtl number and the aspect ratio of inner cylinder diameter (D_i) to the gap width (L).

In the convection problem between two cylinders, the surface of the cylinders can have isothermal (Dirichlet B.C.) or heat flux condition (Neumann B.C.). The previous studies have concentrated the main attention on the annuli with isothermal walls kept at constant wall temperature difference. The problem with Neumann boundary condition generally require the more computation time than that with Dirichlet condition. However, the annulus with constant heat flux on the wall has an important physical aspect, because it can approximate the direct electrical heating by the joule effect. Heat generated by constant electric current in the cylinder creates a constant heat flux condition on the surface of the cylinder (Casterjon and Spalding, 1988). To date, only a few (Van de Sande and Hamer, 1979; Glakpe *et al.*, 1986; Kumar, 1988; Castrejon and Spalding, 1988) have investigated the convection with heat flux boundary conditions; and they did not find multiple solutions. On the other hand, multiple steady solutions were found for an annulus with isothermal walls (Yoo, 1999).

This study investigates the natural convection in a horizontal annulus with constant heat flux on the inner wall. We consider an annulus with a small-diameter inner cylinder ($D_o/D_i = 5$), and investigate transition of flows for various fluids ($0.1 \leq Pr \leq 1$), The annulus considered here approximates an apparatus consisted of an electrically-heated inner rod mounted concentrically within an outer cylinder. A hysteresis phenomenon and dual solutions are found by using numerical analysis. The characteristics of the flow fields, bifurcation phenomena, and distributions of local temperature and heat flux on the walls are investigated.

2. Governing equations and numerical method

The fluid is contained between two horizontal concentric circular cylinders (Figure 1). The surface of hot inner cylinder is maintained at a constant heat flux (q_H), and the cold outer cylinder is kept at a constant temperature (T_o). The Boussinesq approximated dimensionless 2D. Governing equation can be written as follows (Kumar, 1988; Yoo, 1998):

$$\frac{\partial \omega}{\partial t} = J(\Psi, \omega) + Pr\nabla^2\omega - PrRa\left[\sin(\phi)\frac{\partial \theta}{\partial r} + \cos(\phi)\frac{\partial \theta}{r\partial \phi}\right] \tag{1}$$

$$\omega = -\nabla^2\Psi \tag{2}$$

$$\frac{\partial \theta}{\partial t} = J(\Psi, \theta) + \nabla^2\theta \tag{3}$$

where the Jacobian $J(F,G)$ and Laplacian ∇^2 are defined as

$$J(F, G) = \frac{1}{r}\left(\frac{\partial F}{\partial r}\frac{\partial G}{\partial \phi} - \frac{\partial F}{\partial \phi}\frac{\partial G}{\partial r}\right) \tag{4}$$

$$\nabla^2 = \frac{\partial}{r\partial r}\left(r\frac{\partial}{\partial r}\right) + \frac{\partial^2}{r^2\partial \phi^2} \tag{5}$$

The boundary conditions on the walls are

$$\Psi = \frac{\partial \Psi}{\partial r} = 0, \quad \omega = -\frac{\partial^2 \Psi}{\partial r^2}, \quad \frac{\partial \theta}{\partial r} = -1 \quad \text{at } r = r_i \tag{6}$$

$$\Psi = \frac{\partial \Psi}{\partial r} = 0, \quad \omega = -\frac{\partial^2 \Psi}{\partial r^2}, \quad \theta = 0 \quad \text{at } r = r_o \tag{7}$$

The flow is assumed symmetric about the vertical plane through the center of cylinders.

We define the average heat transfer coefficient ($\bar{h}$) with, the mean temperature ($T_{m,i}$) of the inner cylinder as

$$\bar{h} = \frac{q_H}{(T_{m,i} - T_o)} \tag{8}$$

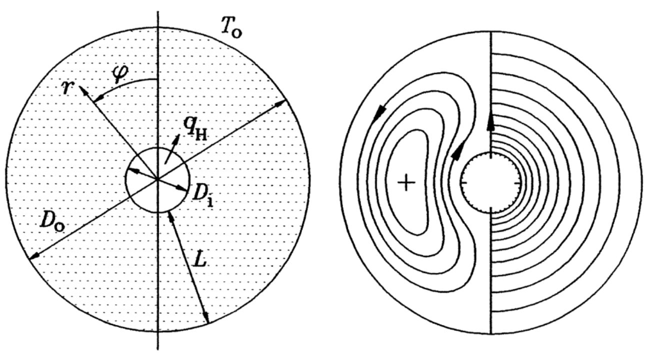

Figure 1.
Problem configuration and a plot of streamlines and isotherms of conduction-dominated regime

The mean Nusselt number ($\overline{\mathrm{Nu}}$) can be

$$\overline{\mathrm{Nu}} = \frac{\bar{h}L}{k} = \frac{1}{\theta_{\mathrm{m,i}}} \tag{9}$$

The local heat flux (q_{o}) on the outer cylinder is given by

$$\frac{q_{\mathrm{o}}}{q_{\mathrm{H}}} = -\frac{\partial \theta}{\partial r} \quad \text{at} \quad r = r_{\mathrm{o}} \tag{10}$$

The unsteady governing equations (1)-(7) are numerically solved by using finite difference method. Equations (1) and (3) are cast into finite difference form using the leap-frog method of Dufort-Frankel for the diffusion and time derivative terms, and central differencing for the Jacobian (Roache, 1972). The derivative terms, and central differencing for the Jacobian (Roache, 1972). The Poisson equation for the streamfunction is discretized by use of five-point formula, and the discretized equation is solved by the direct method of Buzbee *et al.* (1970). A uniform grid spacing is used in the angular direction, and the following coordinate stretching is utilized in the radial direction.

$$r = r_{\mathrm{i}} + \frac{1}{2}\left[1 + \frac{\tanh\{C(2\eta - 1)\}}{\tanh(C)}\right] \quad \text{with } C = 1.5, \quad 0 \leq \eta \leq 1 \tag{11}$$

We consider an annulus with $D_{\mathrm{o}}/D_{\mathrm{i}} = 5$, and use a $(r \times \phi)$ mesh of (65×65) : mesh test has been made, and the (65×65) mesh was confirmed to give sufficiently accurate result (Table I).

3. Results and discussion

Computations were performed for the fluids with $0.1 \leq Pr \leq 1$ in the range of $Ra \leq 3 \times 10^5$. At first, we investigate the transition phenomena with $Pr = 0.1$. Figure 2 shows the variation of flow fields with respect to Ra for $Pr = 0.1$. The conduction dominated flow at small Ra constitutes a kidney-shaped eddy in a half annulus which is nearly symmetric about the horizontal axis of $\phi = \pi/2$, and the most strong fluid flow

Angular direction				
$(r \times \phi)$ mesh	35×33	35×65	35×129	35×257
ϕ, $\overline{\mathrm{Nu}}$				
$\phi_{t,\max}$ (°)	60.0	62.6	63.1	63.2
$\phi_{q,\max}$ (°)	55.2	57.2	57.7	57.9
$\phi_{S,i}$ (°)	48.1	50.1	50.6	50.7
$\phi_{S,o}$ (°)	52.1	53.4	53.7	53.8
$\bar{\mathrm{Nu}}$	5.73	5.82	5.84	5.84
Radial direction				
$(r \times \phi)$ mesh	25×65	45×65	65×65	85×65
ϕ, $\overline{\mathrm{Nu}}$				
$\phi_{t,\max}$ (°)	62.7	62.5	62.4	62.4
$\phi_{q,\max}$ (°)	56.9	57.3	57.4	57.5
$\phi_{S,i}$ (°)	50.5	50.0	49.9	49.9
ϕ (°) $_{S,o}$	53.3	53.5	53.5	53.5
$\bar{\mathrm{Nu}}$	5.79	5.83	5.85	5.86

Table I. Test of grid spacings in the angular and radial directions with the locations of maximum temperature ($\phi_{t,\max}$), maximum heat flux ($\phi_{q,\max}$), and separation points ($\phi_{\mathrm{S,i}}$, $\phi_{\mathrm{S,o}}$), and mean Nusselt number ($\bar{\mathrm{Nu}}$) for $Pr = 0.1$ with $Ra = 1.5 \times 10^5$,

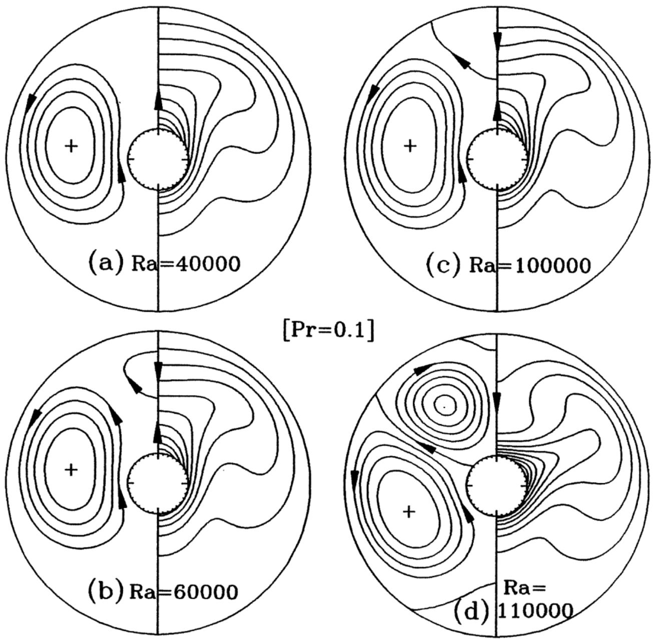

Figure 2.
Streamlines and isotherms showing the transition sequence of flows with respect to Ra at $Pr = 0.1$, (a) $Ra = 4 \times 10^4$, (b) $Ra = 6 \times 10^4$, (c) $Ra = 10^5$, (d) $Ra = 1.1 \times 10^5$, the cross " + " in the flow field indicates the point of $\Psi_{\max}$

occurs in the vertical section of the annulus (Figure 1). As Ra increases, the rising fluid near hot inner cylinder tends to flow in the upward vertical direction, and the fluid flow along the wall becomes relatively weak, since the viscosity of the fluid is too small to drag the fluid along the inner wall when $Pr = 0.1$; and consequently the fluid on the upper part of the annulus becomes relatively stagnant (Figure 2(a): $Ra = 4 \times 10^4$). The relatively stagnant zone on the upper part of the annulus becomes wide with increase of Ra, and finally a new weak eddy is created in that zone due to the horizontal temperature gradient and the dragging effect of the large eddy at $5 \times 10^4 \leq Ra \leq 7 \times 10^4$ (Figure 2(b)). As Ra increases further, the weak eddy grows and extends to the outer cylinder at $8 \times 10^4 \leq Ra \leq 10^5$ (Figure 2(c)), and afterwards extends to the inner cylinder at $Ra = 1.1 \times 10^5$ (Figure 2(d)).

Figure 2 shows four kinds of flow patterns, but we can classify the flow patterns into two classes according to the flow direction atop the inner cylinder. We can see that the fluid near the top of hot inner cylinder moves upward in the flow fields of Figure 2(a)-(c), but moves downward in Figure 2(d). We will name the former as an "upward flow" and the latter as a "downward flow"; then Figure 2 shows a transition of flows from upward to downward flow with increase of Ra. However, it was observed that if we used the downward flow of Figure 2(d) as an initial condition, the same type of flow was also obtained at the values of Ra's in Figure 2(a)-(c). Examples of the downward flows thus obtained are shown in Figure 3 for $Ra = 4 \times 10^4$ and 6×10^4. In other words, Figures 2(a) and (b) and 3(a) and (b) show dual flows at $Ra = 4 \times 10^4$ and 6×10^4 for the fluid with $Pr = 0.1$.

We have investigated the transition phenomena of flows systematically by increasing and decreasing Ra, and the results for $Pr = 0.1$ are shown in Figure 4.

The figure shows mean Nusselt number and bifurcation of flows as functions of *Ra*. As *Ra* increases, a transition from upward to downward flow occurs at an upper critical *Ra* ($Ra_{cU} \approx 1.05 \times 10^5$); and a transition form downward to upward flow occurs at a lower critical *Ra* ($Ra_{cL} \approx 3.8 \times 10^4$) by decreasing *Ra*. A hysteresis phenomenon occurs between the two solution branches of upward and downward flows, and flows exist at $Ra_{cL} < Ra < Ra_{cU}$. When there exist dual flows at $Pr = 0.1$, the mean Nusselt number of downward flow is greater that that of upward flow.

Figure 5 shows the distributions of temperature on inner cylinder and local heat flux on outer cylinder for $Pr = 0.1$ with $Ra = 4 \times 10^4$ and 10^5. For the upward flows, the maximum temperature on the inner cylinder always occurs at the uppermost point of the cylinder ($\phi = 0$), but the heat flux on the outer cylinder has its maximum value at the point other than $\phi = 0$ when $Ra = 4 \times 10^4$ and 10^5, and the location of the point is varied with *Ra*. This fact can be also seen from the flow fields and shapes of the thermal plume in Figure 2. For the downward flows, both the maximum temperature and maximum heat flux occur, at $\phi \neq 0$.

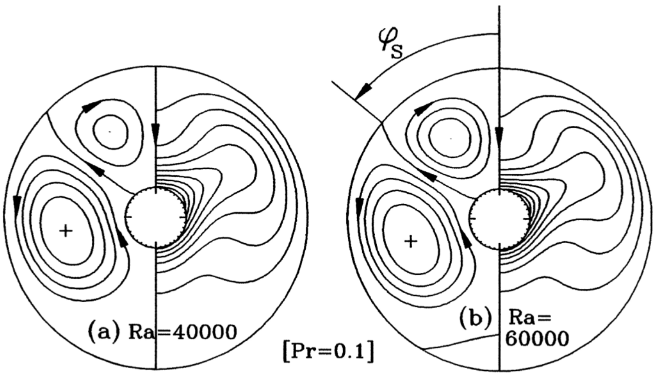

Figure 3. Downward flows at $Pr = 0.1$, (a) $Ra = 4 \times 10^4$, (b) $Ra = 6 \times 10^4$. The angle ϕ_S represents the location of separation point on the wall

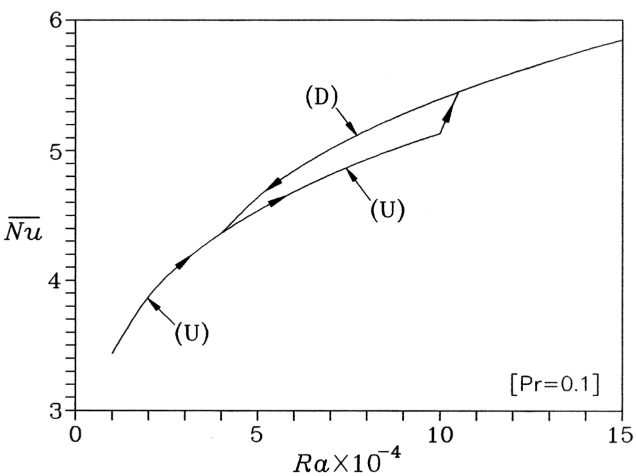

Figure 4. Mean Nusselt number (Nū) as a function of *Ra* for $Pr = 0.1$. The letters "U" and "D" denote the "upward" and "downward" flows, respectively. The transition phenomena with respect to *Ra* are represented with arrows on the curve of Nū

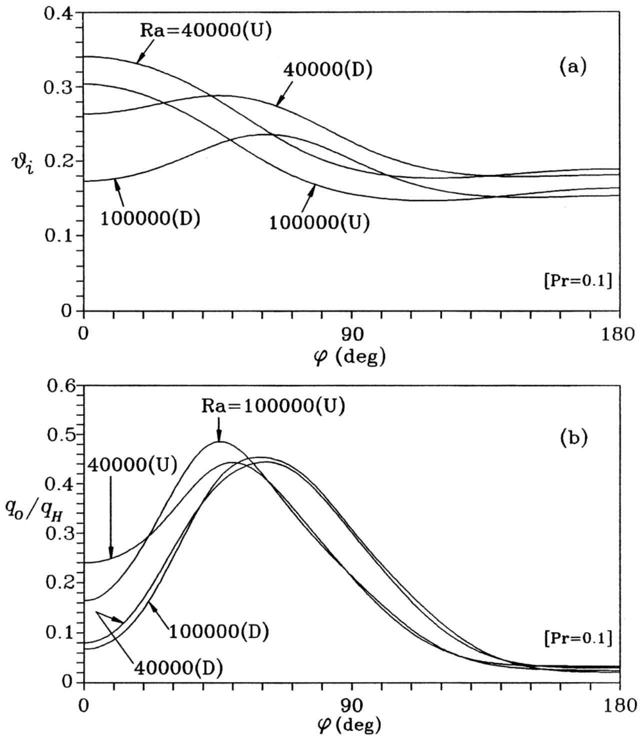

Figure 5.
Distributions of temperature and heat flux of dual solutions on the walls for $Pr = 0.1$ with $Ra = 4 \times 10^4$ and 10^5, (a) local temperature distribution on the inner cylinder $[\theta_i(\phi)]$, (b) local heat flux distribution on the outer cylinder $[q_o(\phi)/q_H]$. The letters "U" and "D" denote the "Upward" and "downward" flows, respectively

The locations of maximum heat flux ($\phi_{q,\max}$), maximum temperature ($\phi_{t,\max}$) and separation points on inner($\phi_{S,i}$) and outer ($\phi_{S,o}$) cylinders, as functions of Ra for $Pr = 0.1$ are shown in Figure 6. For upward flow, $\phi_{q,\max} = 0$ at the conduction dominated regime of $Ra \leq 1,500$, but $\phi_{q,\max} > 0$ at $Ra \geq 2,000$ and increases rapidly with increase of Ra up to $Ra \approx 2 \times 10^4$ at which $\phi_{q,\max}$ has its maximum value ($\approx$51.1°); and afterwards $\phi_{q,\max}$ decreases with increase of Ra, and finally a transition from upward to downward flow occurs at about $\phi_{q,\max} = \pi/4$. For downward flow, the point of maximum temperature on the inner cylinder is shifted upward ($\phi_{t,\max}$ decreases) as Ra decreases, and it is notable that a reverse transition form downward to upward flow occurs when the point is near $\pi/4$. The separation points (Figure 3) of two cells at the inner and outer cylinder always locate above the points of maximum temperature and maximum heat flux, respectively, $\phi_{S,i} < \phi_{t,\max}$ on inner cylinder, and $\phi_{S,o} < \phi_{q,\max}$ on outer cylinder. And $\phi_{t,\max}$, $\phi_{S,i}$, and $\phi_{S,o}$ show nearly identical behavior with respect to Ra.

The points of maximum temperature and maximum heat flux on, the walls are important in engineering applications. We have tested several meshes by varying the grid numbers in the radial and angular directions to determine the accurate locations of the points (Table I). We can see that the ($r \times \phi$) mesh of (65×65) yields sufficiently accurate results for the present problem. When using a much finer mesh of (65×257) at $Pr = 0.1$ and $Ra = 1.5 \times 10^5$, the values of $\phi_{t,\max}$, $\phi_{q,\max}$, $\phi_{S,i}$, $\phi_{S,o}$, and $\overline{\mathrm{Nu}}$ are, 63.1, 58.2, 50.5, 53.9, and 5.87°, respectively. The errors of $\phi_{t,\max}$ and $\phi_{q,\max}$ between (65×65) and (65×257) meshes, are about 1.1 and 1.4 percent, respectively.

We have observed that the transition phenomenon from upward to downward flow found for the fluid of $Pr = 0.1$ does not occur, when $0.2 \leq Pr \leq 1$. For the fluid of $0.2 \leq Pr \leq 1$, the transient development of flows starting from zero initial condition ($\omega = \theta = 0$) or the upward flow of lower Ra yields upward flow for all Ra. However, if we use the downward flow of $Pr = 0.1$ as an initial condition, the same type of downward flow can be obtained for $0.2 \leq Pr \leq 1$ above a certain critical Rayleigh number.

Figure 7 shows an example of the dual flows of $Pr = 0.2$ at $Ra = 10^5$, and the mean Nusselt number and bifurcation phenomenon of $Pr = 0.2$ are shown in Figure 8. When $Pr = 0.2$, the ascending fluid flow in the top part of the annulus is strong, and a stagnant zone is not formed in that region (Figure 7), and consequently, transition form upward to downward flow does not occur (Figure 8). Only the transition from downward to upward flow occurs at a critical Ra, by decreasing Ra; and dual flows exist above the critical Ra (Figure 8). In the regime of dual flows at $Pr = 0.2$, the mean Nusselt number of upward flow is greater than that of downward flow (Figure 8), which is an opposite behavior to those of $Pr = 0.1$ (Figure 4).

Figure 9(a)-(c) shows the locations of maximum heat, flux ($\phi_{q,\max}$) on the outer cylinder and maximum temperature ($\phi_{t,\max}$) on the inner, wall as functions of Ra, when

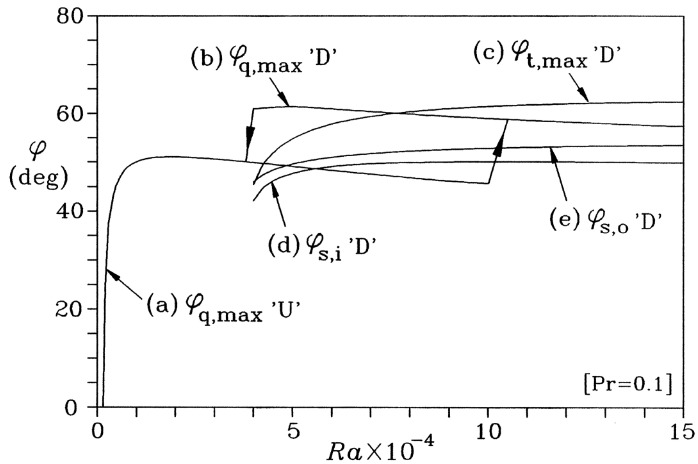

Figure 6. Angles representing the locations of maximum heat, flux ($\phi_{q,\max}$), maximum temperature ($\phi_{t,\max}$), and separation points ($\phi_{S,i}$, $\phi_{S,o}$) on the walls, when $Pr = 0.1$, (a), (b) $\phi_{q,\max}$, (c) $\phi_{t,\max}$, (d) $\phi_{S,i}$, (e) $\phi_{S,o}$. The letters "U" and "D" denote the "upward" and "downward" flows, respectively. All the the angles are measured from the top of annulus (Figure 1)

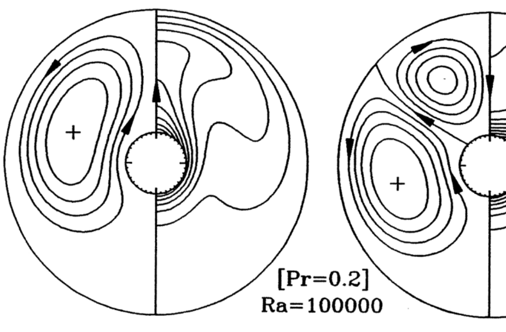

Figure 7. Streamlines and isotherms of dual flows when $Pr = 0.2$ and $Ra = 10^5$

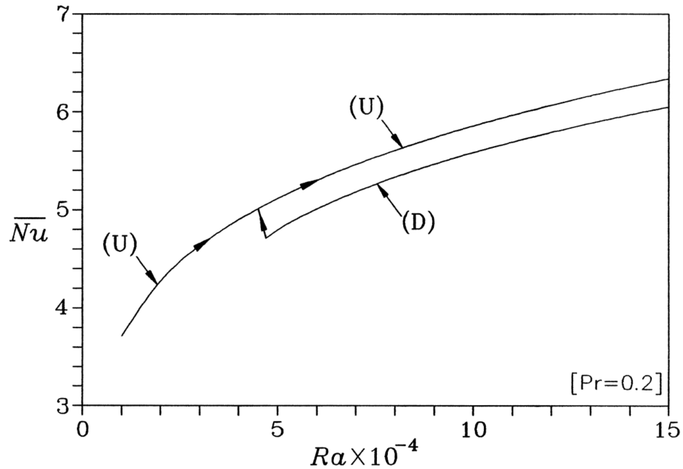

Figure 8.
Mean Nusselt number (Nū) as a function of *Ra* when $Pr = 0.2$. The letters "U" and "D" denote the "upward" and "downward" flows, respectively

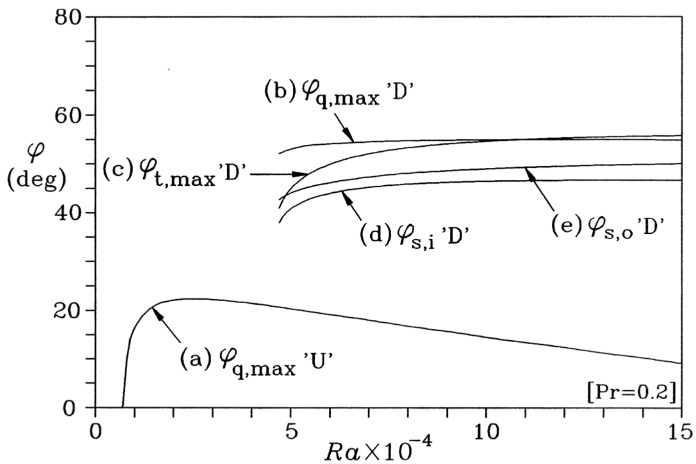

Figure 9.
Angles representing the, locations maximum heat flux ($\phi_{q,\max}$), maximum temperature ($\phi_{t,\max}$), and separation points ($\phi_{S,i}$, $\phi_{S,o}$) on the walls, when $Pr = 0.2$, (a), (b) $\phi_{q,\max}$, (c) $\phi_{t,\max}$, (d) $\phi_{S,i}$, (e) $\phi_{S,o}$. The letters "U" and "D" denote "upward" and "downward" flows, respectively

$Pr = 0.2$. Although the upward flow of $Pr = 0.2$ can have its maximum heat flux at the point other than $\phi = 0$, the ratio of [max (q_o)]/[q_o(at $\phi = 0$)] is <1.05 for an *Ra*; and the maximum value of $\phi_{q,\max}$ is about 22° (Figure 9(a)), which is much smaller than that of $Pr = 0.1$ (Figure 6(a)). For the downward flow of $Pr = 0.2$, the temperature on the inner cylinder and the heat flux on the outer cylinder at high *Ra* have their maximum values at the nearly the same angular positions (Figure 9(b) and (c)). The behavior of the locations of separation points ($\phi_{S,i}$, $\phi_{S,o}$) with respect to *Ra* shown in Figure 9(d) and (e) for $Pr = 0.2$ is similar to that of $Pr = 0.1$. However, $Pr = 0.2$ has the smaller values of $\phi_{S,i}$ and $\phi_{S,o}$ than $Pr = 0.1$, at the same *Ra*: that is, the separation points are shifted upward more than the case of $Pr = 0.1$.

It has been observed that the upward flow of $0.3 \leq Pr \leq 1$ has both the maximum temperature on inner cylinder and the maximum heat flux on outer cylinder, at $\phi = 0$. An example of dual flows in $0.3 \leq Pr \leq 1$ is shown in Figure 10 with $Pr = 0.7$ (air), and the corresponding distributions of temperature and heat flux on the walls are shown in Figure 11. As Pr increases, the center of the main eddy moves upward, for both upward and downward flows (Figures 7 and 10). The mean Nusselt number characteristics of dual flows and bifurcation phenomenon at $0.3 \leq Pr \leq 1$ are the same as those of $Pr = 0.2$ shown in Figure 8.

Up to now, we have investigated the transition phenomena of flows for various fluids at $0.1 \leq Pr \leq 1$, and observed duel steady flows which are dependent on Pr and Ra. The solution regimes are summarized on the $Pr - Ra$ plane in Figure 12. The flow of $Pr = 0.1$ has one steady flow at $Ra < Ra_{cL}$ and $Ra > Ra_{cU}$, but has dual steady flows at $Ra_{cL} < Ra < Ra_{cU}$. When $0.2 \leq Pr \leq 1$, dual flows exist at $Ra > Ra_c$. The critical Rayleigh number above which dual flows exist is increased, as Pr increases.

4. Conclusions

We have considered a two-dimensional natural convection problem in a horizontal annulus with a small-diameter inner cylinder ($D_o/D_i = 5$) subjected to a constant heat flux condition. And the transition phenomena are investigated for various fluids with $0.1 \leq Pr \leq 1$.

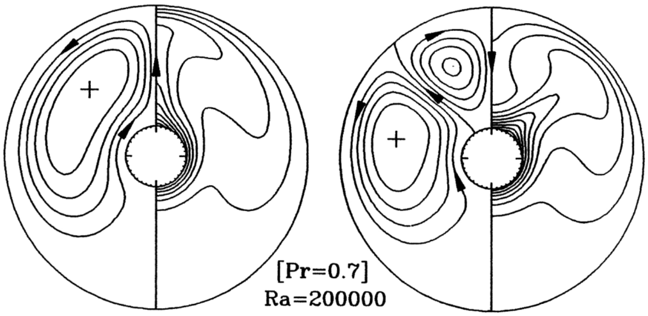

Figure 10. Streamlines and isotherms of dual flows when $Pr = 0.7$ and $Ra = 2 \times 10^5$

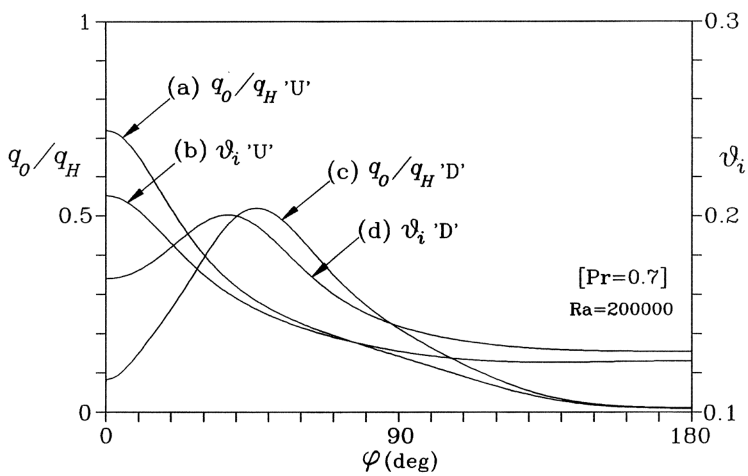

Figure 11. Distributions of heat flux $[q_o(\phi)/q_H]$ on the outer cylinder and temperature $[\theta_i(\phi)]$ on the inner cylinder for $Pr = 0.7$ with $Ra = 2 \times 10^5$, (a) $q_o(\phi)/q_H$ "U", (b) $\theta_i(\phi)$ "U", (c) $q_o(\phi)/q_H$ "D", (d) $\theta_i(\phi)$ "D". The letters "U" and "D" denote the "upward" and "downward" flows, respectively

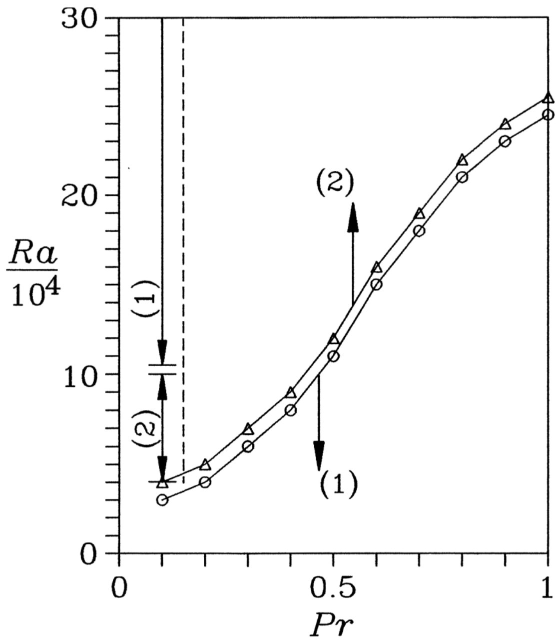

Figure 12.
Solution regimes on the $Pr - Ra$ plane. The numbers in the parentheses represent the number of solutions. The marks "△" and "○" indicate the calculation points at which two solutions and one solution are found, respectively. The curve of Ra_c lies between the two boundary curves of "△" and "○"

We classify the flow patterns largely into two classes according to the flow direction atop the hot inner cylinder: an "upward flow" and a "downward flow". At $0.1 \leq Pr \leq 1$, dual steady-state solutions of upward and downward flows are found. A hysteresis phenomenon occurs at $Pr = 0.1$, but only a transition from downward to upward flow occurs at $0.2 \leq Pr \leq 1$. At $Pr = 0.1$, the mean Nusselt number of downward flow is larger than that of upward flow; but when $0.2 \leq Pr \leq 1$, downward flow has the less mean Nusselt number than upward flow. Downward flow has its maximum temperature and maximum heat flux on the walls at the point other than the uppermost point of the cylinders ($\phi = 0$). For the upward flow, maximum heat flux on the outer cylinder occurs at $\phi \neq 0$ at high Ra, when $0.1 \leq Pr \leq 0.2$; but it occurs at $\phi = 0$ for all Ra, when $0.3 \leq Pr \leq 1$. As Pr increases, the critical Rayleigh number above which dual exist is increased.

References

Busse, F.H. (1981), "Transition to turbulence in Rayleigh-Bénard convection", in Swinney, H.L. and Gollub, J.P. (Eds), *Topics in Applied Physics*, Vol. 45, Springer, New York, NY, pp. 97-137.

Buzbee, B.L., Golub, G.H. and Nielson, C.W. (1970), "On direct methods for solving Poisson's equations", *SIAM J. Numer. Analysis*, Vol. 7, pp. 627-56.

Castrejon, A. and Spalding, D.B. (1988), "An experimental and theoretical study of transient free-convection flow between horizontal concentric cylinders", *Int. J. Heat Mass Transfer*, Vol. 31 No. 2, pp. 273-84.

Gebhart, B., Jaluria, Y., Mahajan, R.L. and Sammakia, B. (1988), *Buoyancy-induced Flows and Transport*, Hemisphere Publishing Corporation, New York, NY, pp. 764-71.

Glakpe, E.K., Watkins, C.B. Jr. and Cannon, J.N. (1986), "Constant heat flux solutions for natural convection between concentric and eccentric horizontal cylinders", *Numerical Heat Transfer*, Vol. 10 No. 3, pp. 279-95.

Kuehn, T.H. and Goldstein, R.J. (1976), "An experimental and theoretical study of natural convection in the annulus between horizontal concentric cylinders", *J. Fluid Mech.*, Vol. 74, pp. 695-719.

Kumar, R. (1988), "Study of natural convection in horizontal annuli", *Int. J. Heat Mass Transfer*, Vol. 31 No. 6, pp. 1137-48.

Lee, Y. and Korpela, S.A. (1983), "Multicellular natural convection in a vertical slot", *J. Fluid Mech.*, Vol. 126, pp. 91-121.

Roache, P.J. (1972), "Computational fluid dynamics", *Hermosa*, pp. 53-64.

Van de Sande, E. and Hamer, B.J.G. (1979), "Steady and transient natural convection in enclosures between horizontal circular cylinders (constant heat flux)", *Int. J. Heat Mass Transfer*, Vol. 22 No. 3, pp. 361-70.

Yoo, J-S. (1998), "Natural convection in a narrow horizontal cylindrical annulus: $Pr \leq 0.3$", *Int. J. Heat Mass Transfer*, Vol. 41 No. 20, pp. 3055-73.

Yoo, J-S. (1999), "Prandtl number effect on bifurcation and dual solutions in natural convection in a horizontal annulus", *Int. J. Heat Mass Transfer*, Vol. 42 No. 17, pp. 3279-90.